A crustal model along 39°S from a seismic refraction profile-ISSA 2000

Stefan Lüth

Freie Universität Berlin, Fachrichtung Geophysik,
Malteserstr. 74-100, 12249 Berlin, Germany
e-mail: stefan@geophysik.fu-berlin.de

Peter Wigger

Freie Universität Berlin, Fachrichtung Geophysik,
Malteserstr. 74-100, 12249 Berlin, Germany
e-mail: wigger@geophysik.fu.berlin.de

ISSA Research Group: Manuel Araneda[2], Günter Asch[3], Klaus Bataille[4], Mirjam Bohm[3], Carsten Bruhn[5], Peter Giese[1], Stefan Lüth[1], Jorge Quezada[4], Andreas Rietbrock[5], Peter Wigger[1].

[1] Freie Universität Berlin, Fachrichtung Geophysik, Germany; [2] SEGMI, Santiago de Chile; [3] GeoForschungsZentrum Potsdam, Germany; [4] Universidad de Concepción, Chile; [5] Universität Potsdam, Germany.

ABSTRACT

The results of a seismic refraction profile across the Southern Andes at 39°S from the Chilean Pacific coast to the Argentinean Neuquén Basin are presented here. A 2-D crustal velocity model was derived from traveltime forward modeling of the correlated phases on shot-sections from shot-points in the Pacific Ocean and in the Chilean Main Cordillera. The crustal velocity model is characterized by lower average velocities in the fore-arc than in the arc. A typical continental Moho was not observed under the fore-arc, under the arc the Moho could only be inferred from teleseismic receiver function studies. The oceanic Moho was observed down to *ca.* 45 km depth under the continental fore-arc. Using additional structural and seismic data, the velocity model was extrapolated to the west and to the east, and this model was converted into a rough density model. The gravity, computed from this density model, is consistent with the free-air and Bouguer gravity. A crustal thickness of *ca.* 40 km is inferred for the magmatic arc. Gradually decreasing average velocities of the continental crust from east to west are proposed to be due to the influence of the intrusion of the North Patagonian batholith in the east and of decreasing age of the accretionary wedge together with underplating of subducted sediments at the base of the continental crust in the west.

Key words: Seismic refraction, Crustal structure, Southern Chile.

RESUMEN

Un modelo de la corteza a lo largo de los 39°S derivado de un perfil de sísmica de refracción-ISSA 2000. En este estudio se presentan los resultados de un perfil sísmico de refracción a través de los Andes meridionales a los 39°S desde la costa pacífica chilena hasta la cuenca de Neuquén, Argentina. Un modelo cortical 2D de velocidad se obtuvo del modelamiento directo del tiempo recorrido de las fases correlacionadas con las secciones de disparos

desde los 'shot points' en el Océano Pacífico y en la Cordillera Principal chilena. El modelo cortical de velocidad está caracterizado por velocidades medias más bajas en el antearco que en el arco. No se observó un Moho continental bajo el antearco, bajo el arco se pudo inferir el Moho solamente por estudios telesísmicos de las funciones del receptor. El Moho oceánico fue observado bajo *ca.* 45 km de profundidad bajo el antearco continental. Al usar datos estructurales y sísmicos adicionales, el modelo de velocidad fue extrapolado al oeste y al este, y convertido en un modelo aproximado de densidad. La gravedad, calculada desde este modelo de densidad, es consistente con la anomalía de aire libre y la de Bouguer. Se deduce un grosor cortical de *ca.* 40 km para el arco magmático. Se proponen velocidades medias de la corteza continental que disminuyen gradualmente desde el este al oeste, los cuales se deben a la influencia de la intrusión del batolito nordpatagónico por el este y de edades decrecientes de la cuña acrecionaria junto con la subplaca de los sedimentos subducidos en la base de la corteza continental en el oeste.

Palabras claves: Refracción sísmica, Estructura de la corteza, Sur de Chile.

INTRODUCTION

The Andean belt has been built by magmatic and tectonic processes related to the subduction of oceanic lithosphere (Nazca-Plate) beneath the South American continent. Whereas in the Central Andes these processes resulted in an extremly thickened continental crust with more than 70 km thickness (Giese *et al.*, 1999; Romanyuk *et al.*, 1999; Schmitz *et al.*, 1999), the crust of the Southern Andes (south of 37°S) has remained relatively thin and in general shows low elevations below 2,000 m (*e.g.*, Lowrie and Hey, 1981). Neither a plateau formation like the Altiplano-Puna plateau nor a broadening of the orogenic belt occurred in the southern Andes.

The largest earthquake ever recorded occurred in the fore-arc region of the investigated area. The city of Valdivia and its surrounding region were most severely damaged by a series of earthquakes on May 21 and 22, 1960. The main shock exceeded Mw=9.5. The rupture length of the earthquake series is estimated to be up to 1,000 km, starting at about 38°S and extending to the south (Cifuentes, 1989). This earthquake and the presence of a long seismic gap north of the rupture area (Beck *et al.*, 1998) possibly indicating a strongly increased seismic hazard in the region of the city of Concepción have motivated many geoscientific investigations in that area.

The German Collaborative Research Center (SFB) 267 *Deformation Processes in the Andes* carried out many geoscientific investigations in the southern central Andes, in northern Chile, south-west Bolivia and north-west Argentina. Among them are several seismic refraction and reflection profiles (*e.g.*, ANCORP Working Group, 1999) and local seismological networks (*e.g.*, Haberland and Rietbrock, 2001). In order to extend the seismic image of the Chilean continental margin to an area where a basically similar plate-tectonic framework as in northern Chile did not result in an orogen as gigantic as in the Central Andes but seismicity is characterized by even stronger events than in the north, an integrated seismological experiment was carried out in southern Chile and Argentina (Fig. 1). The experiment consisted of passive seismological recordings and a seismic refraction profile. In this contribution the authors present the evaluation of the seismic refraction measurements along a transect at 39°S. The resulting velocity model and gravity observations are used in order to extrapolate the crustal structure along the transect.

TECTONIC AND GEOLOGICAL SETTING

The seismic transect crossed, from west to east, the Coastal Cordillera, the Longitudinal Valley, and the Main Cordillera, and reached the Neuquén Basin in the back-arc (Fig. 1). The basement underneath the western part of the profile has been built by a Permo-Triassic accretionary wedge. This complex consists of low grade metamorphic slates and greenstones. The Meso-Cenozoic North

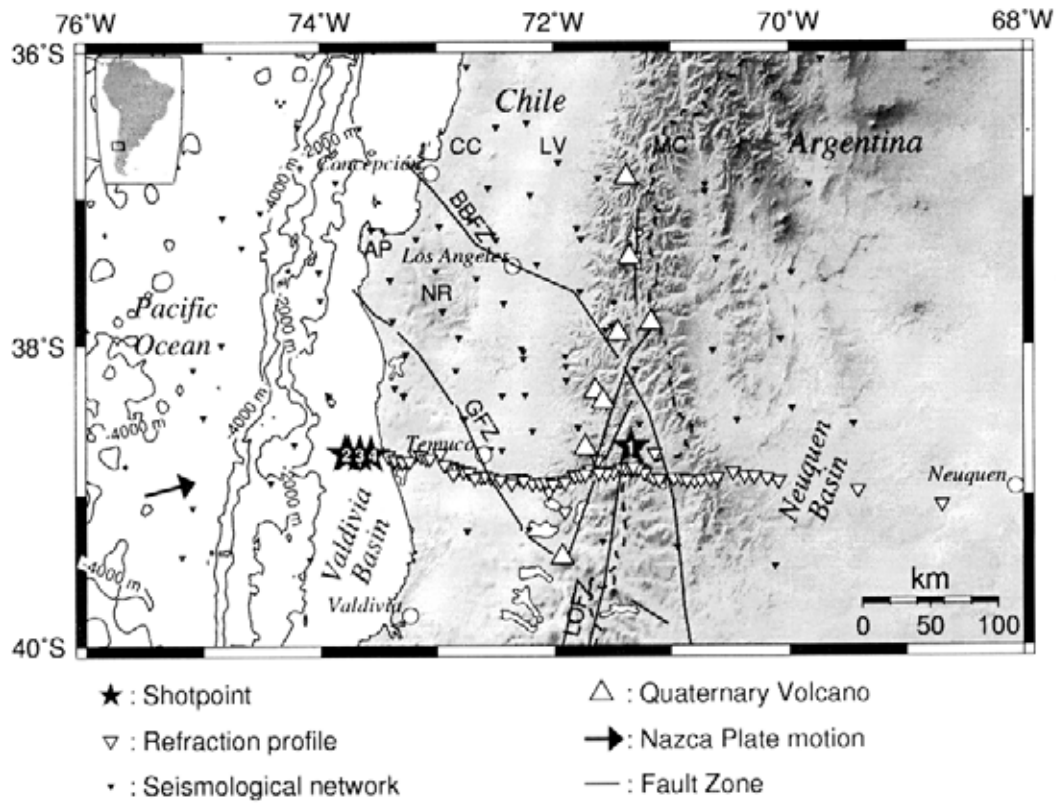

FIG. 1. Map of the ISSA 2000 measurements in Chile and Argentina. Black stars with numbers indicate the shot points. White inverted triangles denote the locations of the receivers of the refraction profile. The station distribution of the local seismological network is indicated by small black inverted triangles. Convergence direction (black arrow) after DeMets *et al.*, 1990; **LOFZ**- Liquiñe Ofqui Fault Zone; **GFZ**- Gastre Fault Zone; **BBFZ**- Biobío Fault Zone; **CC**- Coastal Cordillera; **LV**- Longitudinal Valley; **MC**- Main Cordillera; **AP**- Arauco Peninsula; **NR**- Nahuelbuta Mountain Range. Geometry of fault zones from D. Melnick (oral communication, 2002).

Patagonian Batholith intruded the crust thus building up the Main Cordillera of the southern Andes (Hervé, 1994). In the Coastal Cordillera and Longitudinal Valley, the basement is overlain by intercalations of volcanic rocks and marine and nonmarine sediments of late Oligocene to middle Miocene age and Quaternary sediments. The volcanic rocks are known as the Mid-Tertiary Central Valley and Coastal Magmatic Belt (Jordan *et al.*, 2001 and references therein).

The present magmatic arc consists of a chain of andesitic to basaltic stratovolcanos, some of which are located along a prominent north-south trending lineament defined by the Liquiñe Ofqui Fault zone (LOFZ). From Pliocene/early Pleistocene to late Quaternary the volcanic front migrated 30-80 km westward to its present position (Muñoz and Stern, 1989). The LOFZ is a major dextral strike slip fault zone extending more than 1,100 km from the vicinity of the Istmo de Ofqui into the lake region, at approximately 38°S (Cembrano *et al.*, 2000). It has been active, at least, since the Eocene, either resulting from oblique subduction of the Nazca Plate under the South American continent (Hervé, 1994; Lavenu and Cembrano, 1999), or from the indenter effect of the Chile Ridge at the southern termination of the fault system (Nelson *et al.*, 1994). In the magmatic arc Pliocene to Quaternary volcanic rocks lie over a volcanic and sedimentary unit known as the Cura-Mallín Formation dating from early to middle Miocene (Jordan *et al.*, 2001).

The continental fore-arc between 36 and 40°S is split into segments with different metamorphic and magmatic histories related to Pre-Andean orogeny. The boundaries between these segments are defined by the Gastre and Biobío fault zones (Rapela

and Pankhurst, 1992; Melnick *et al.*, 2002). The Gastre and Liquiñe Ofqui faults are characterized by enhanced electrical conductivity at depths between 20 and 40 km suggesting that these are continental scale fault zones (Brasse and Soyer, 2001). The Gastre and Biobío fault zones are connected with crustal seismicity indicating their activity whereas the crustal block between them, consisting of the Arauco Peninsula and Nahuelbuta Mountain Range, is nearly devoid of any seismicity (Bohm *et al.*, 2002).

East of the Andean Cordillera the Neuquén Basin, a large ensialic basin, developed during Jurassic and early Cretaceous showing active Quaternary volcanism (Mpodozis and Ramos, 1989). This basin is the southern part of the Andean Basin, a Pacific oriented backarc basin which had been controlled by thermal subsidence up to Late Cretaceous, thereafter additionally sediment load subsidence occurred (Leanza *et al.*, 2000). The Neuquén Basin is filled by a sedimentary succession which is up to 7 km thick and mainly originating from the magmatic arc (Riccardi *et al.*, 2000; Eppinger and Rosenfeld, 1996).

THE SEISMIC EXPERIMENT

The integrated seismic experiment consisted of three parts, the first of which started in May 1999. Within this part broad band receivers were deployed along a transect at 39°S and on a north-south profile along the Pacific coast. The stations were operating from May 1999 to November 2001. The remaining two parts of the integrated seismic experiment were realized in the first four months of the year 2000. They consisted of a local seismological network recording local seismicity in the area and a seismic refraction line (Fig. 1).

The 320 km long seismic refraction profile consisted of 65 stations with an average spacing of 4-5 km. The authors used 3-component Mark L4-3D 1 Hz, Lennartz LE-3D 1 Hz seismometers, and Guralp 5 s broadband seismometers. For data logging PDAS, MarsLite, Guralp, and Orion recorders were used. The stations recorded continuously at a 10 ms sampling rate. As a time reference the signal of the Global Positioning System (GPS) was used. The time of the shots was determined by recordings of the electric ignition impulses of the explosions using a GPS-based system.

Five chemical explosions were shot, one from a point in a small lake in the Chilean Main Cordillera (SP 1) and four from points in the Pacific Ocean (SP 2.1, 2.2, 3, 4). The coordinates and charges of the shots are listed in table 1. The shots in the Pacific Ocean were realized with the RV Kay Kay belonging to the Oceanographic Department of the Universidad de Concepción. Four shots at distinct locations in the Pacific Ocean were fired instead of only one in order to enhance the resolution of lateral velocity variations and dip-angles of layer boundaries. If, *e.g.*, phase correlations of the oceanic *PmP*-phase are available on several consecutive shots, a 2-D model with a dipping oceanic Moho can be derived with a relatively small trade-off between average velocity and dip-angle of the reflecting interface. If only one shot section with *PmP*-correlations is available and the reverse shot does not show any *PmP*-onsets, the trade-off between velocity above the reflector and its dip-angle cannot be resolved.

TABLE 1. SHOTLIST OF THE SEISMIC REFRACTION EXPERIMENT IN THE ISSA 2000 PROJECT.

List of shotpoints No.	Location	Elevation (m)	Charge (kg)	Date and time
1	71°20'29.7"W 38°41'05.8"S	1100	120	23.01.2000 12:15:47.45
2.1	73°47'18.5"W 38°43'38.4"S	-122	200	22.04.2000 13:22:44.03
2.2	73°45'36.8"W 38°43'40.9"S	-110	200	22.04.2000 15:02:09.50
3	73°39'47.3"W 38°43'47.2"S	-76	80	22.04.2000 16:53:25.12
4	73°33'52.9"W 38°44'00.1"S	-46	200	22.04.2000 18:30:05.38

Shot 1 is located in the Main Cordillera, shots 2.1 to 4 were fired at the sea bottom in the Pacific Ocean.

MAIN FEATURES OF THE VELOCITY MODEL

The detailed treatment of the seimic data which led to the construction of the 2D P-wave velocity model of the southern Andes (Fig. 2) are found in Appendix 1.

Three main features can be derived from the velocity model which proved to be stable throughout the model assessment:

- In the upper 20 km the crust shows a lateral heterogeneity with lower average velocity in the fore-arc (6.1 km/s for the uppermost 20 km) than in the arc (6.4 km/s for the uppermost 20 km). The upper crust, defined by v_p between 5.9 and 6.4 km/s is, roughly 10 km thick underneath the magmatic arc where high velocities (about 6.8 km/s) are reached at shallow depth. Underneath the fore-arc the upper crust is 15 km thick and lower velocities (v_p = 6.5-6.6 km/s) are found at its base. This feature has not been assessed by the 1-D perturbation test, however it is necessary to explain the different apparent velocities observed for the *LC* phase in shots 1 from the Main Cordillera and 2, 3, 4 from the Pacific Ocean.
- The lower crust, marked by P-wave velocities of more than 6.5 km/s, starts at ~11 km depth under the arc and ~15 km depth under the coastal cordillera, and thickens from 10 to 20 km from the fore-arc to the arc. Underneath the fore-arc its lower boundary is constrained by a very diffuse *PmP(1)* phase, whereas under the magmatic arc only receiver function studies give a hint that the continental Moho is at about 40 km depth (X. Yuan, oral communication, 2001).
- Between the lower continental crust and the layer boundary inferred from the *PmP(2)* phase a wedge-shaped structure with v_p = 6.9-7.3 km/s underneath the fore-arc is present. A velocity inversion within it, which would be geometrically consistent with the crust of the subducting oceanic plate, is possible, but not necessary, to explain the data because the upper boundary of this inversion layer is not directly represented by a phase in the data. Whereas the upper eastern part of this layer can be obviously attributed to the continental mantle (which is supposed to be below 40 km deep under the arc), this is not the case for the upper western part where P-wave velocity appears to be considerably lower than typical for mantle.

INTEGRATED CRUSTAL MODEL ALONG 39°S FROM SEISMOLOGY AND GRAVITY

Further hints on whether the velocity model is realistic can be drawn from a comparison of the gravity of the derived density model with observed gravity.

In order to extend the narrow area, where the crustal structure at depths below 20 km can be derived from the seismic data, the P-wave velocities and some other structural data were used to build a crustal model for the whole subduction zone from the Nazca Plate to the Argentine Neuquén Basin. The geometry of the offshore part of the model is derived from seafloor topography and seismic reflection data (Bangs and Cande, 1997). For the v_p of the oceanic crust and mantle the nearest wide-angle velocity model available has been used (Flüh *et al.*, 1998). The velocity distribution as derived from the ISSA observations was extrapolated west and eastward for the continental crust. The only free parameter which had to be adjusted in order to 'fit' the modeled gravity with the observed gravity, was the depth of the Moho under the magmatic arc.

For conversion of the velocities to density values, a linear relationship after Ludwig *et al.* (1970) valid for sedimentary rocks was used for lower velocities (below 6.1 km/s). The distribution of velocity-density values is shown in figure 3.

At greater depths the linear relation between velocity and density becomes irregular due to the effect of pressure and temperature (*e.g.*, Sobolev and Babeyko, 1994). For velocity values greater than 6.1 km/s a three steps procedure is followed in order to account for the pressure and temperature dependence of the velocity-density relation (Kirchner, 1997; Döring, 1998). First, using the in situ P-wave velocity, the velocity at normal pressure and temperature is determined. Secondly, this

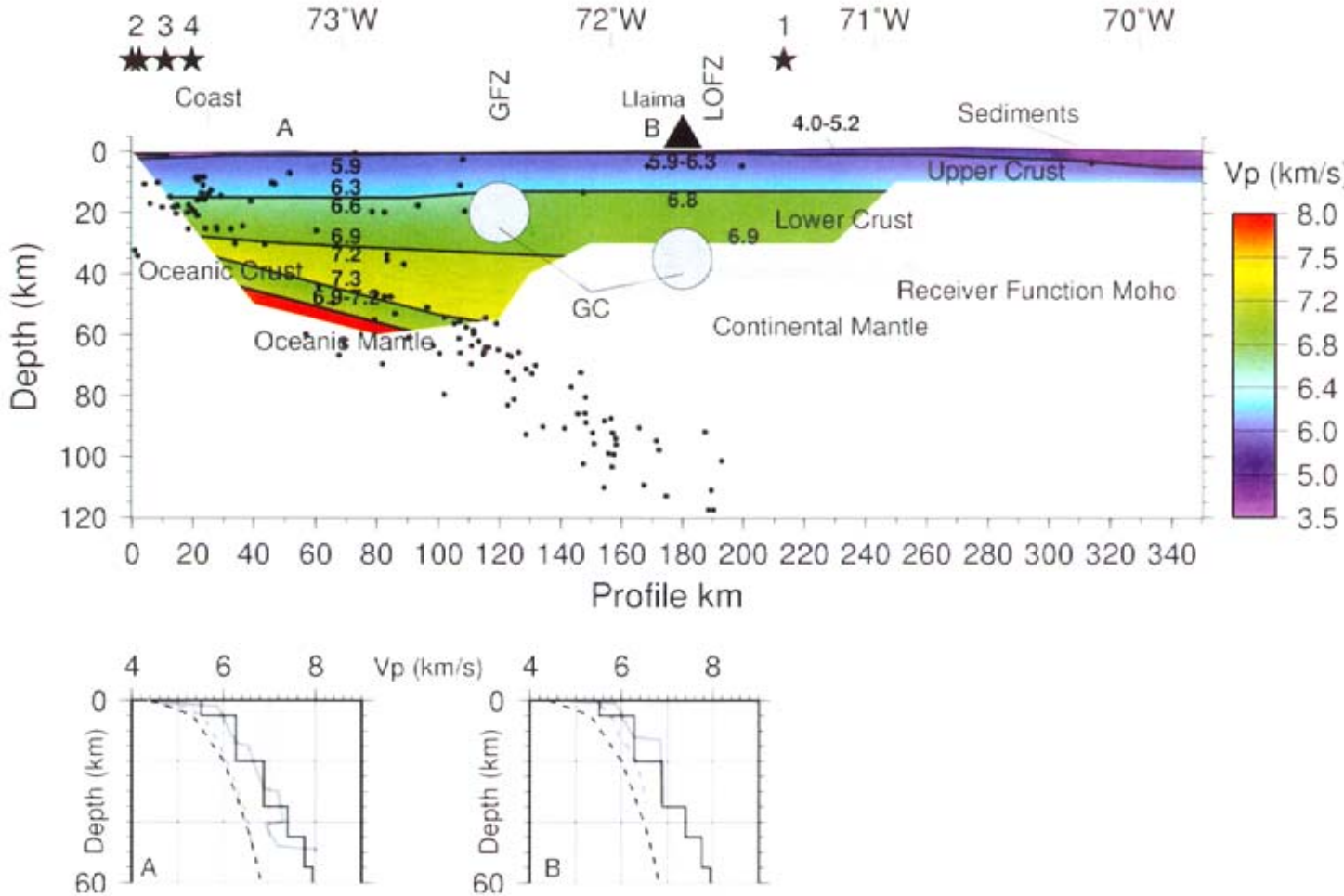

FIG. 2. P-wave velocity model as derived from iterative traveltime modeling. The velocity model is represented by color coding and values given near the layer boundaries (thick black lines). Black dots indicate the earthquake hypocenters located from the ISSA passive seismological experiment (Bohm *et al.*, 2002). The hypocenters have been projected perpendicularly onto the model plane. Only events south of 37° S are shown. The position of the receiver function Moho is according to X. Yuan (oral communication, 2001). Grey circular patches at 120 km and 180 km indicate locations of good electrical conductors (GC) after Brasse and Soyer (2001). The diagrams below the section show velocity-depth functions for representative locations along the profile in the fore-arc (A) and the magmatic arc (B). Thick grey line: interval velocity of the model from seismic refraction; thin black line: 1-D velocity model from passive seismology; grey dashed line: average velocity of the model from seismic refraction; black dashed line: average velocities of the 1-D velocity model from passive seismology. **GFZ**- Gastre Fault Zone; **LOFZ**- Liquine-Ofqui Fault Zone.

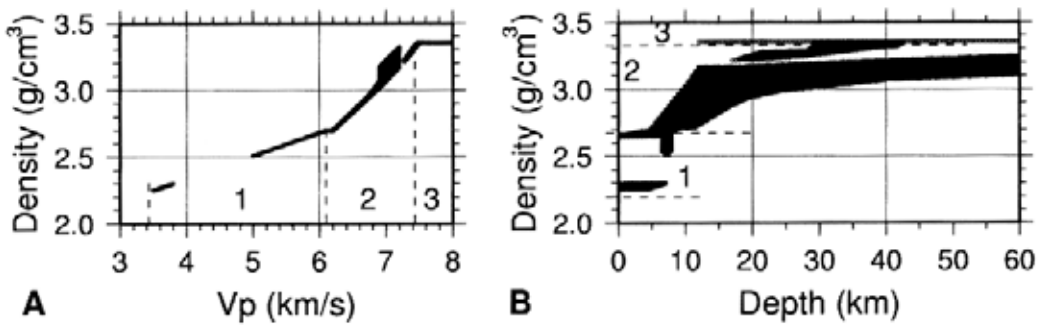

FIG. 3. **A-** Crossplot of the velocity-(rho) density relations. A linear relation was used for sediments with P-wave velocities from 3.4 to 6.1 km/s (area 1 in the plots). For higher velocities, a three steps procedure was used (see text for description and references). The result is a basically linear relation (area 2 in the plots). Only for velocities of about 7 km/s the curve broadens. This broadening is due to the large depth range (approximately 10 to 60 km) of the oceanic crust. With increasing depth, higher densities are computed for the same velocity than for shallow depths. A constant density of 3.35 g/cm³ was used for the mantle (area 3 in the plots); **B-** Distribution of density with respect to depth. Maximum depth of low densities (less than 2.5 g/cm³) is reached at the trench. The great maximum depth of density values less than 3.35 g/cm³ is due to the oceanic crust. Oceanic and continental mantle is represented by an average density of 3.35 g/cm³ which is distributed from 12 to 60 km depth.

velocity is used to compute density at normal conditions. The density is, thirdly, converted into in situ density. The resulting density model is then used to model the gravity along the transect. For comparison with free-air (offshore) and Bouguer (onshore) gravity (Götze *et al.*, 2001) the modeled gravity is shifted such that the gravity values at the station above the trench are identical. The comparison between the modeled and measured gravity (Fig. 4) shows that the density model derived from the extended velocity along the transsect explains the regional trend of the gravity. The contrast between the gravity low at the trench and the gravity high at the coast is explained except for a local discrepancy at 200 profile-km. This part of the integrated model is not covered by our seismic data. A possible explanation for the discrepancy between modeled and measured gravity is, that the velocity model assumes too high P-wave velocities for the offshore part of the continental crust. A reduction of the P-wave velocity at 200 profile-km would result in lower density and thus lower gravity there. In order to resolve this, a better coverage of seismic data west of the ISSA transect is necessary which is provided by the offshore-onshore experiment SPOC carried out from September 2001 through January 2002 (BGR, 2002). The gravity low between 400 and 500 profile-km (70.5° to 71.5°W) is well explained by a crust of about 40 to 45 km maximum thickness. This model can only be a very rough estimation of the real velocity and density distribution, particularly east and west of the part covered the seismic refraction profile. However, the velocity model, the used velocity-density relation, and the measured relative gravity along the transect are basically consistent with each other.

DISCUSSION AND CONCLUSIONS

A 2-D P-wave velocity model of the Southern Andes determined from seismic refraction measurements at 39°S has been presented. The model, reaching from the Pacific coast to the Argentinian Neuquén Basin, is characterized by slower average velocities in the fore-arc crust than in the crust of the magmatic arc. A continental Moho under the arc was only observed using teleseismic earthquakes and the receiver function imaging technique (X. Yuan, oral communication, 2001). The oceanic Moho was observed by the seismic refraction profile down to *ca.* 45 km under the coastal cordillera. While magneto-telluric measurements along the transect yielded good conductors correlating with prominent

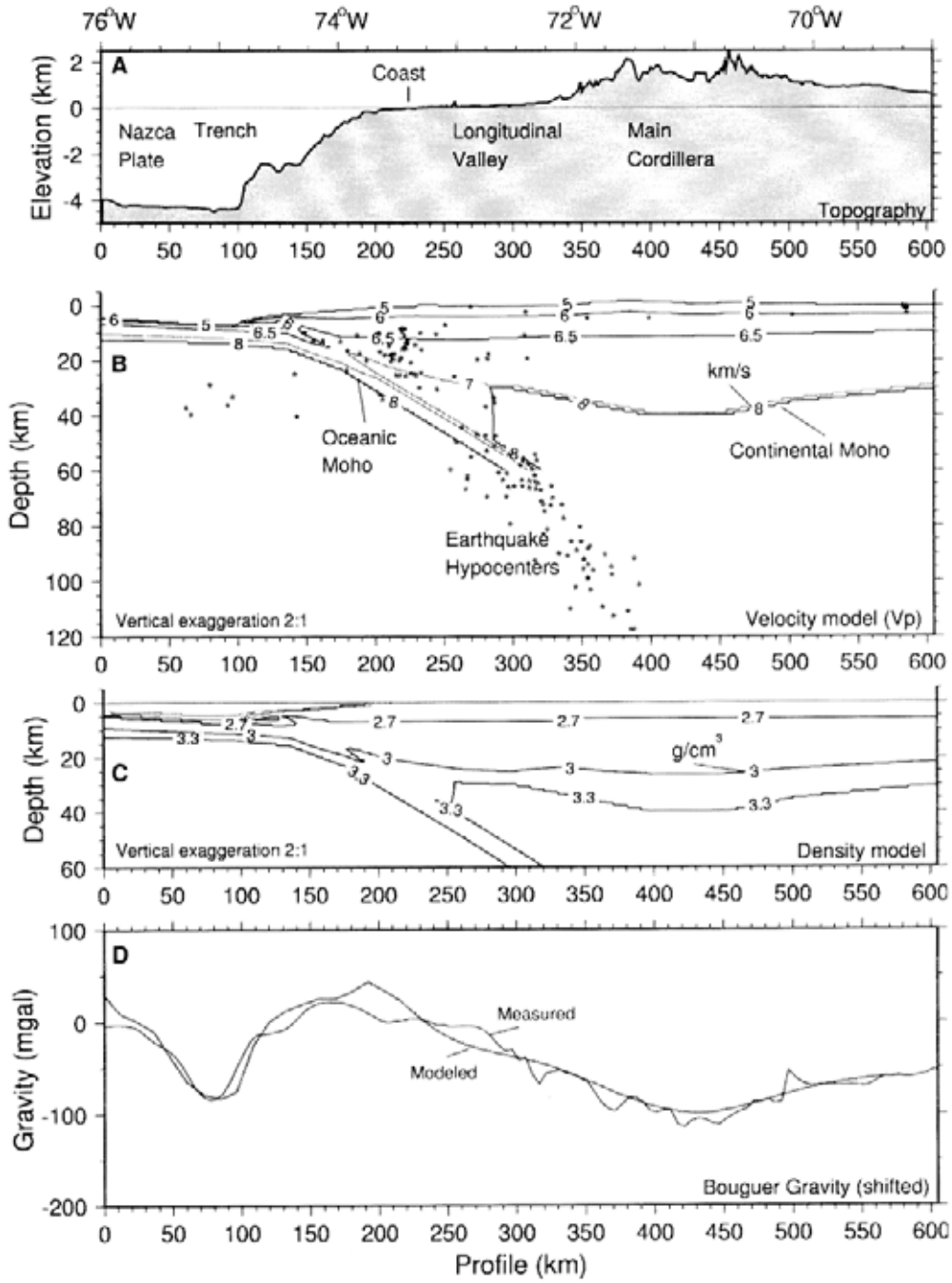

FIG. 4. **A**- Seafloor and surface topography; **B-** velocity model with earthquake hypocenters; **C-** density model derived from velocity model, and **D-** comparison of free-air/Bouguer gravity (Götze *et al.*, 2001) and modeled gravity along a transect at 39°S from 76°W to 69° W. Free-air and Bouguer gravity values were vertically shifted for the comparison with the computed gravity.

fault zones at the surface (GFZ, LOFZ), the velocity model, as far as could be resolved by the sparse shot geometry, is basically uncorrelated with these fault zones. Higher P-wave velocities of the arc-crust may be indicative of the influence of the intruded North Patagonian Batholith which is considered to be responsible for a higher metamorphic grade there than in the fore-arc, which is not influenced by the intrusion (Herve, 1994). The smooth velocity increase not typical for a continental Moho under the continental fore-arc at approx. 30 km depth is either due to the presence of strongly hydrated and serpentinized mantle, or due to subducted meta-sediments which are being underplated at the base of the continental crust. Uplift which is observed in parts of the coastal area (Bohm *et al.*, 2002) may be an additional hint for relatively light (and thus seismically slow) material being underplated. Based on sand box modeling, this area is the postulated center of basal accretion and antiformal stacking at depth (Lohrmann *et al.*, 2000).

Based on the ISSA velocity model a rough model (Fig. 4B) of the southern Chilean subduction zone is proposed. This model was converted into a rough density model (Fig. 4C), the gravity answer of which was compared with free-air and Bouguer gravity along the transect Fig. 4D). There is a generally good correlation between measured and computed gravity except for some small scale anomalies which are not taken into account by this rough model. A clear discrepancy west of the coast indicates lower density (and thus lower P-wave velocities) in the offshore continental crust. The magmatic arc is characterized by a roughly 40 km thick crust, which corresponds to the world average of a continental arc (Christensen and Mooney, 1995). To the east of the magmatic arc, increasing gravity suggests that the crust becomes thinner by about 5 km.

For comparison, in figure 5 the velocity model of the southern central Andes at 21 S is shown (ANCORP Working Group, JGR in press). The basic differences between the transects are:

- A 20 to 30 km greater crustal thickness in the magmatic arc of the central Andes than in the south.
- Lower crustal average P-wave velocities in the arc than in the fore-arc in the central Andes (Wigger *et al.*, 1994), viceversa in the southern Andes. These differences are due to the completely different

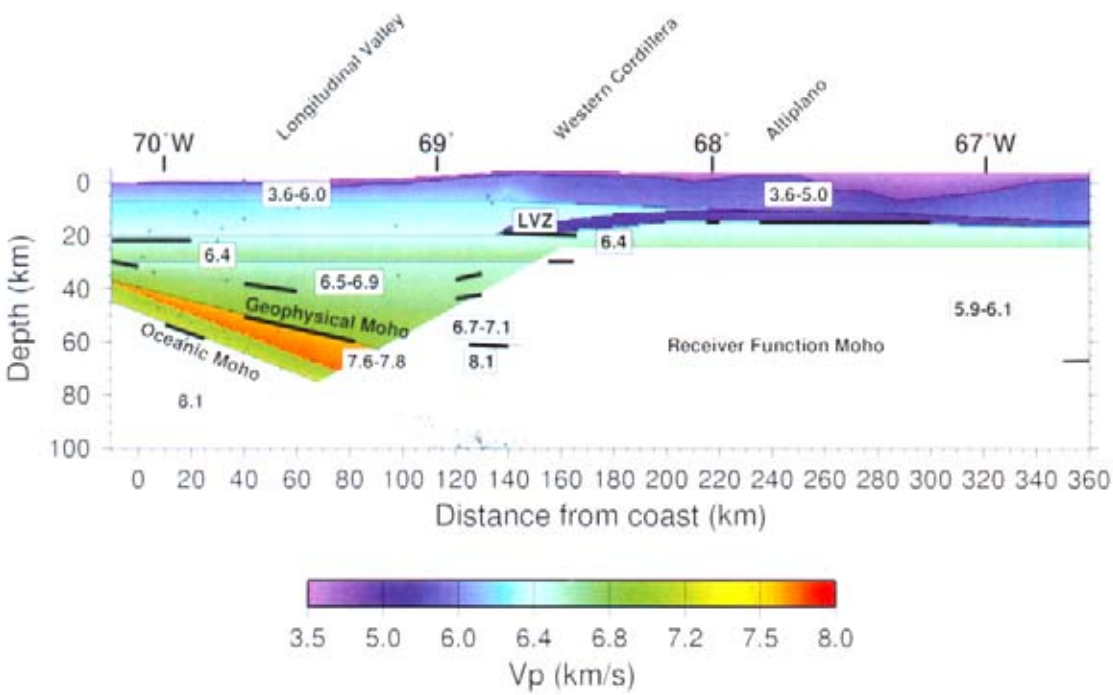

FIG. 5. Velocity model from the southern central Andes along 21° S (ANCORP Working Group, in press). The receiver Function Moho is according to Yuan *et al.*, 2001.

development of the continental crust during the Andean cycle. In the central Andes, frontal erosion at the trench since the Jurassic resulted in an eastward migration of the volcanic front of about 200 km (Scheuber *et al.*, 1994). What is now fore-arc crust, was magmatic arc in Jurassic and Early Cretaceous times. The original (oceanic and continental) crust of the present fore-arc had been replaced to a large extent by plutonic and volcanic rocks (Scheuber *et al.*, 1994). These rocks are responsible for high seismic velocities observed by refraction profiles there whereas the active magmatism in the arc is not only connected with high heat flow (Springer and Förster, 1998), high seismic attenuation (Haberland and Rietbrock, 2001) and electric conductivity (Echternacht *et al.*, 1997), but also with the presence of seismic low-velocity-zones and thus lower average velocity values. Contrary to this, in the southern Andes there has been no considerable migration of the magmatic arc Hervé, 1994; Jordan *et al.*, 2001). East-west variations of magmatic activity during the Andean cycle are due to changes on subduction rate and obliquity (Jordan *et al.*, 2001). After the late Paleozoic accretionary complex had been built up, which is representing most of the continental fore-arc crust, there was little change in the subduction geometry. The gradually decreasing crustal seismic velocities from east to west reflect the decreasing age of the accretionary complex and increasing tectonic activity towards the west due to subducted sediments being underplated at the base of the continental crust.

ACKNOWLEDGEMENTS

The seismic experiment was financed by the German Science Foundation (DFG) in the frame of the Collaborative Research Center (SFB) 267 and by the German Ministry of Science and Education and Ministry of Economy and Technology (BMBF and BMWT), grant 03G0545A/1. The authors are grateful for organizational support by Universidad de Concepción, Departamento de Ciencias de la Tierra and Departamento de Oceanografía, particularly Captain M. Monné and the crew of the research vessel Kay Kay. Field work was carried out by the authors and with the committed help of coworkers from several institutions: G. Aguilera, J. L. Cerda, J. Oliva (Universidad Católica del Norte, Antofagasta, Chile); G. Astroza, L. Caric, I. Cartes, E. Carvacho, M. Escobar, S. Jara, G. Lacazette, C. Leal, R. Mora, L. Parra, S. Pérez (Universidad de Concepción, Chile); J. Avila, A. Canales (Universidad de Chile, Santiago); B. Heit (Universidad Nacional de Salta, Argentina); D. Chalbaud (Universidad Simón Bolivar, Caracas, Venezuela); J. Kummerow, J. Saul (GFZ Potsdam, Germany); D. Vollmer (Universität Potsdam, Germany); A. Belmonte, F. Finck, S. Hölz, J. Rindschwentner (Freie Universität Berlin, Germany). Instruments for this experiment were provided by the Geophysical Instrument Pool Potsdam (GIPP) at the GFZ Potsdam, Freie Universtät Berlin, Universität Potsdam and GEOMAR Kiel.

All figures were drafted using the GMT package (Wessel and Smith, 1995). The authors are grateful for constructive remarks from L. Dorbath (Institut Physique du Globe, France), C. Mpodozis (Sipetrol, Chile), G. Yáñez (Codelco-Chile), J. Cañuta (Sernageomin) and an anonymous reviewer.

REFERENCES

Ancorp Working Group. 1999. Seismic reflection image revealing offset of Andean subduction-zone earthquake locations into oceanic mantle. *Nature*, Vol. 397, p. 341-344.

Ancorp Working Group. (In press). Seismic imaging of a convergent continental margin and plateau in the Central Andes (ANCORP'96). *Journal of Geophysical Research.*

Bangs, N.; Cande, S.C. 1997. Episodic development of a convergent margin inferred from structures and processes along the southern Chile margin. *Tectonics*, Vol. 16, No. 3, p. 489-503.

Beck, S.; Barrientos, S.; Kausel, E.; Reyes, M. 1998. Source characteristics of historic earthquakes along the Central Chile subduction zone. *Journal of South American Earth Sciences*, Vol. 11, No. 2, p. 115-129.

Bundesanstalt für Geowissenschaften und Rohstoffe Hannover (BGR). 2002. Cruise Report Sonne Cruise SO-161 Leg 2 and 3. *Bundesanstalt für Geowissenschaften und Rohstoffe*, 145 p. Hannover, Germany.

Bohm, M.; Lüth, S.; Asch, G.; Bataille, K.; Bruhn, C.; Rietbrock, A.; Wigger, P. 2002. The Southern Andes between 36°S and 40°S latitude: seismicity and average velocities. *Tectonophysics*, Vol. 356, p. 275-289.

Brasse, H.; Soyer, W. 2001. A magnetotelluric study in the Southern Chilean Andes. *Geophysical Research Letters*, Vol. 28, No. 19, p. 3757-3760.

Cembrano, J.; Schermer, E.; Lavenu, A.; Sanhueza, A. 2000. Contrasting nature of deformation along an intra-arc shear zone, the Liquiñe Ofqui fault zone, southern Chilean Andes. *Tectonophysics*, Vol. 319, p. 129-149.

Christensen, N.I.; Mooney, W.D. 1995. Seismic velocity structure and composition of the continental crust: a global view. *Journal of Geophysical Research*, Vol. 100, p. 9761-9788.

Cifuentes, I.L. 1989. The 1960 Chilean earthquake. *Journal of Geophysical Research*, Vol. 94, p. 665-680.

Díaz-Naveas, J.L. 1999. Sediment Subduction and Accretion at the Chilean Convergent Margin Between 35° S and 40°S. Ph.D. Thesis (Unpublished), *Christian Albrechts-Universität zu Kiel*, 130 p.

DeMets, C.; Gordon, R.G.; Argus, D.F.; Stein, S. 1990. Current plate motions. *Geophysical Journal International*, Vol. 101, No. 2, p. 425-478.

Döring, J. 1998. Dichteverteilung und Modellierung des isostatischen Verhaltens der Lithosphäre im Südural. *Berliner Geowissenschaftliche Abhandlungen*, Vol. (B) 29, 136 p.

Echternacht, F.; Tauber, S.; Eisel, M.; Brasse, H.; Schwarz, G.; Haak, V. 1997. Electromagnetic study of the active continental margin in northern Chile. *Physics of the Earth Planetary Interiors*, Vol. 102, p. 69-88.

Eppinger, K.J.; Rosenfeld, U. 1996. Western margin and provenance of sediments of the Neuquén Basin (Argentina) in the Late Jurassic and Early Cretaceous. *Tectonophysics*, Vol. 259, p. 229-244.

Flüh, E.R.; Vidal, N.; Ranero, C.R.; Hojka, A.; von Huene, R.; Hinz, K.; Cordoba, D.; Dañobeitia, J.J.; Zelt, C. 1998. Seismic investigation of the continental margin off and onshore Valparaíso, Chile. *Tectonophysics*, Vol. 288, p. 251-263.

Giese, P.; Scheuber, E.; Schilling, F.; Schmitz, M.; Wigger, P. 1999. Crustal thickening processes in the central Andes and the different natures of the Moho-discontinuity. *Journal of South American Earth Sciences*, Vol. 12, p. 201-220.

Götze, H.-J.; Krause, S.; Romanyuk, T.; Schmidt, S.; Schulte, J.; Tasarova, S.; Wienecke, S. 2001. Density and susceptibility anomalies as an indicator of anomalous p-t conditions. *In* Collaborative Research Center 267, Deformation Processes in the Andes, report for the research period 1999-2001. *Freie Universität Berlin, Technische Univesität Berlin, GeoForschungsZentrum Potsdam, Universität Potsdam*, p. 291-320.

González, E. 1989. Hydrocarbon resources in the coastal zone of Chile. In *Geology of the Andes and Its Relation to Hydrocarbon and Mineral Resources* (Ericksen, G.E.; Cañas, M.T.; Reinemund, J.A.; editors). *Circum-Pacific Council for Energy and Mineral Resources Earth Science Series*, p. 383-404.

Haberland, C.; Rietbrock, A. 2001. Attenuation tomography in the western central Andes: a detailed insight into the structure of a magmatic arc. *Journal of Geophysical Research*, Vol. 106 (B6), p. 11151-11167.

Hervé, F. 1994. The Southern Andes between 39° and 44°S latitude: the geological signature of a transpressive tectonic regime related to a magmatic arc. *In* Tectonics of the Southern Central Andes (Reutter, K.-J.; Scheuber, E.; Wigger, P.J.; editors). *Springer-Verlag*, p. 243-248. Berlin, Heidelberg, New York.

Jordan, T.E.; Burns, W.M.; Veiga, R.; Pángaro, F.; Copeland, P.; Kelley, S.; Mpodozis, C. 2001. Extension and basin formation in the southern Andes caused by increased convergence rate: a mid-Cenozoic trigger for the Andes. *Tectonics*, Vol. 20, No. 3, p. 308-324.

Kirchner, A. 1997. 3D-Dichtemodellierung zur Anpassung des Schwere- und des Schwerepotentialfeldes der zentralen Anden. *Berliner Geowissenschaftliche Abhandlungen*, Vol. (B) 25, 98 p.

Lavenu, A.; Cembrano, J. 1999. Compressional and transpressional stress pattern for Pliocene and Quaternary brittle deformation in fore-arc and intra-arc zones (Andes of Central and Southern Chile). *Journal of Structural Geology*, Vol. 21, p. 1669-1691.

Leanza, H.; Rosenfeld, U.; Volkheimer, W.; Zeiss, A. 2000. Facies Evolution of the Mesozoic Neuquén Basin (Argentina) in Space and Time. *Zeitschrift für Angewandte Geologie*, Vol. SH1, p. 95-102.

Lohrmann, J.; Kukowski, N.; Adam, J.; Echtler, H.; Oncken, O. 2000. Identification of controlling parameters of the accretionary southern Chilean margin (38°-40°S) with analogue models. 17. *Geowissenschaftliches Lateinamerika-Kolloquium, Stuttgart, Profile*, Vol. 18, p. 50.

Lowrie, A.; Hey, R. 1981. Geological and geophysical variations along the western margin of Chile near latitude 33° to 36°S and their relation to Nazca Plate subduction. *In* Nazca Plate; crustal formation and Andean convergence (Kulm La Verne, D.; editors *et al.*). *Geological Society of America, Memoir*, Vol. 154, p. 741-754.

Ludwig, J.; Nafe, J.; Drake, C. 1970. Seismic Refraction. *In* The Sea (Maxwell, A.; editor). *Wiley*, Vol. 4, p. 53-84. New York.

Melnick, D.; Folguera, A.; Rosenau, M.; Echtler, H.; Potent, S. 2002. Tectonics from the northern segment of the Liquiñe-Ofqui Fault System (37°-39°S), Patagonian Andes. *In the International Symposium on Andean Geodynamics (ISAG), No. 5*, p. 413-416.

Mpodozis, C.; Ramos, V. 1989. The Andes of Chile and Argentina. *In* Geology of the Andes and its Relation to Hydrocarbon and Mineral Resources (Ericksen, G.E.;

Cañas, M.T.; Reinemund, J.A.; editors). *Circum-Pacific Council for Energy and Mineral Resources, Earth Science Series,* p. 59-90.

Muñoz, J.; Stern, C.R. 1989. Alkaline magmatism within the segment 38°-39° S of the Plio-Quaternary volcanic belt of the southern South American margin. *Journal of Geophysical Research,* Vol. 794, B4, p. 4545-4560.

Nelson, E.; Forsythe, R.H.; Arit, I. 1994. Ridge collision tectonics in terrane development. *Journal of South American Earth Sciences,* Vol. 7, p. 271-278.

Rapela, C.W.; Pankhurst, R.J. 1992. The granites of northern Patagonia and the Gastre Faults system in relation to the break-up of Gondwana. *In* Magmatism and the Causes of Continental Break-Up (Storey, B.C.; Alabaster, T.; Pankhurst, R.J.; editors). *Geological Society of London,* Special Publications, Vol. 68, p. 209-220.

Riccardi, A.C.; Leanza, H.A.; Damborenea, S.E.; Manceñido, M.O.; Ballent, S.C.; Zeiss, A. 2000. Marine Mesozoic Biostratigraphy of the Neuquén Basin. *Zeitschrift für Angewandte Geologie,* Vol. SH1, p. 103-108.

Romanyuk, T.V.; Götze, H.-J.; Halvorson, P.F. 1999. A density model of the Andean subduction zone. *The Leading Edge,* Vol. 18, No. 2, p. 264-268.

Scheuber, E.; Bogdanic, T.; Jensen, A.; Reutter, K.-J. 1994. Tectonic Development of the North Chilean Andes in Relation to Plate Convergence Since the Jurassic. *In* T ectonics of the Southern Central Andes (Reutter, K.-J.; Scheuber, E.; Wigger, P.J.; editors). *Springer-Verlag,* p. 121-140.

Schmitz, M.; Lessel, K.; Giese, P.; Wigger, P.; Bribach, J.; Graeber, F.; Grunewald, S.; Haberland, C.; Lüth, S.; Röwer, P.; Ryberg, T.; Schulze, A. 1999. The crustal structure of the central Andean fore-arc and magmatic arc as derived from seismic studies - the PISCO 94 experiment in northern Chile (21°-23°S). *Journal of South American Earth Sciences,* Vol. 12, p. 237-260.

Sobolev, S.V.; Babeyko, A.Y. 1994. Modeling of mineralogical composition, density and elastic wave velocities in anhydrous magmatite rocks. *Surveys in Geophysics,* Vol. 15, p. 515-544.

Springer, M.H.; Förster, A. 1998. Heat flow density across the Central Andean subduction zone. *Tectonophysics,* Vol. 291, p. 123-139.

Vergani, G.D.; Tankard, A.J.; Belotti,H.J.; Welsink, H.J. 1995. Tectonic Evolution and Paleogeography of the Neuquén Basin, Argentina. *In* Petroleum Basins of South America (Tankard, A.J.; Suárez, R.; Welsink, H.J.; editors). *American Association of Petroleum Geologists (AAPG), Memoir* 62, p. 383-402.

Wessel, P.; Smith, W.H.F. 1995. New version of the Generic Mapping Tools released. *EOS, Transactions, American Geophysical Union (AGU),* Vol. 76, No. 33, p. 329.

Wigger, P.J.; Schmitz, M.; Araneda, M.; Asch, G.; Baldzuhn, S.; Giese, P.; Heinsohn, W.-D.; Martínez, E.; Ricaldi, E.; Röwer, P.; Viramonte, J. 1994. Variation in the Crustal Structure of the Southern Central Andes Deduced from Seismic Refraction Investigations. *In* Tectonics of the Southern Central Andes (Reutter, K.-J.; Scheuber, E.; Wigger, P.J.; editors). *Springer-Verlag,* p. 23-48.

Yuan, X.; Sobolev, S.V.; Kind, R.; Oncken, O.; Andes Working Group. 2000. Subduction and collision processes in the Central Andes constrained by converted seismic phases. *Nature,* Vol. 408, p. 958-961.

Zelt, C.A.; Ellis, R.M. 1988. Practical and efficient ray tracing in two-dimensional media for rapid traveltime and amplitude forward modeling. *Canadian Journal of Exploration Geophysics,* Vol. 24, p. 16-31.

Zelt, C.A.; Smith, R.B. 1992. Seismic traveltime inversion for 2-D crustal velocity structure. *Geophysical Journal International,* Vol. 108, p. 16-34.

Zelt, C.A.; Hojka, A.M.; Flüh, E.R.; McIntosh, K.D. 1999. 3D simultaneous seismic refraction and reflection tomography of wide-angle data from the central Chilean margin. *Geophysical Research Letters,* Vol. 26, No. 16, p. 2577-2580.

Manuscript received: March 5, 2001; accepted: May 03, 2003.

APPENDIX 1

DATA AND MODEL

DATA

The shot sections observed from the shotpoints are displayed in Figs. 2-4 as well as the synthetic traveltimes, ray-diagrams, and ray-synthetic amplitudes derived from the final model.

SHOT 1

The signal from shotpoint 1 (Fig. 1) in the Main Cordillera was recorded from the Pacific coast, 185 km west of the shotpoint, to the Neuquén Basin, 120 km east of the shotpoint. The first breaks between 70 km offset to the west and 110 km offset to the east have a bulk apparent velocity of 6 km/s. Due to their clear appearance in the seismogram they are

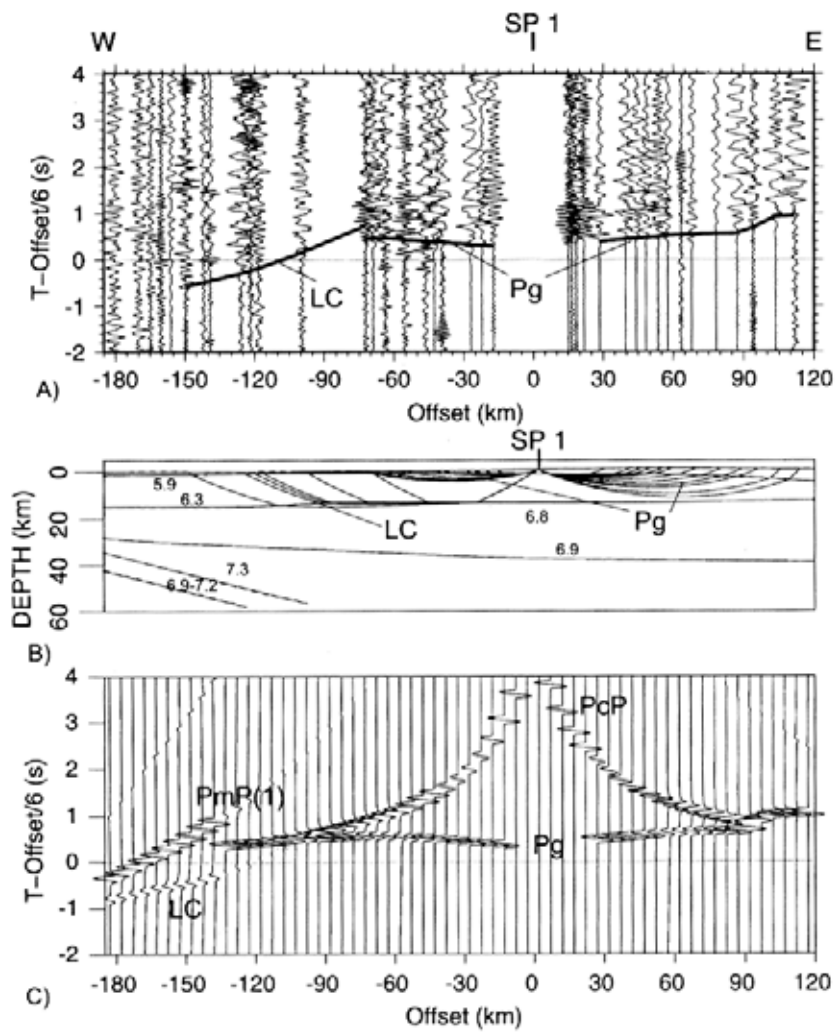

FIG. 1. **A)-** shot section from the shotpoint 1 (Main Cordillera). The data has been bandpass-filtered 4-14 Hz and reduced with 6 km/s. Grey lines denote the modeled traveltimes of the phases which had been picked in the section; **B)-** ray-diagram of the correlated phases. Numbers in the ray-diagram indicate P-wave velocities in km/s. **C)-** ray-theoretical seismogram based on the final velocity model.

interpreted as onsets of the diving wave through the upper crust (Pg). In the east, starting at about 80 km offset, a time delay, interpreted to be caused by increasing sedimentary thickness in the Neuquén Basin, is present. The first breaks in the offset range 185 km to 80 km west of the shotpoint are from a faster diving wave passing the upper margin of the lower crust (LC). The bulk apparent velocity is 6.4 km/s, however the apparent velocity is variable along the section. The modeled section (Fig. 2 bottom) contains clear PcP and PmP(1) arrivals (reflections from the lower crust and continental Moho, respectively). These are not observed in the data, suggesting a rather smooth velocity contrast between upper and lower crust and between lower crust and mantle and/or strong attenuation/scattering in the crust under the arc.

SHOT 2

The section from shot 2.1 is shown in figure 2. The shotpoint is located in the Pacific Ocean, about 30 km off the Chilean coast. Shotpoint 2.2 is about 2.5 km farther east. The section from that shot is basically indentical to that from SP 2.1 so that the authors discuss only SP 2.1. The signal of the shot was recorded from the coast (30 km offset) to the Neuquén Basin (315 km offset). From 30 km to about 120 km the first arrival can be correlated with a bulk apparent velocity of 6

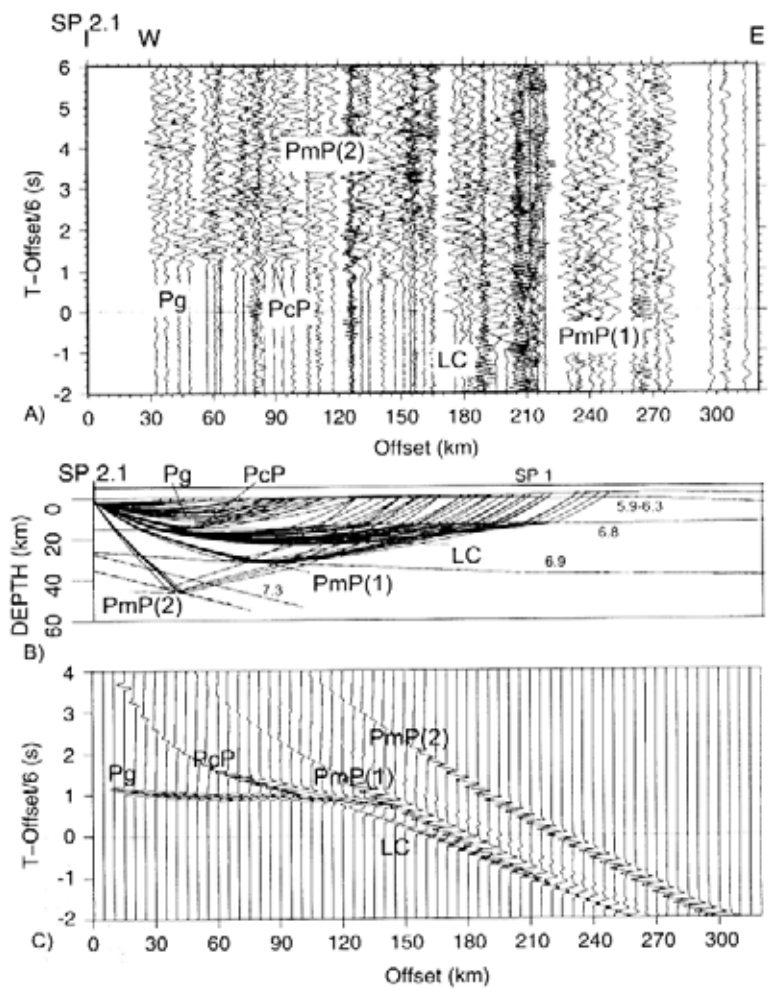

FIG. 2. **A):** shot section from the shotpoint 2.1 (Pacific Ocean). The data have been bandpass-filtered 2-12 Hz and reduced with 6 km/s. Grey lines denote the modeled traveltimes of the phases which had been picked in the section; **B):** ray-diagram of the correlated phases. Numbers in the ray-diagram indicate P-wave velocities in km/s; **C):** ray-theoretical seismogram based on the final velocity model.

km/s (*Pg*). From 120 km to 235 km offset the first arrivals are correlated with an apparent velocity of 7.3 km/s. According to the section of shot 1 these arrivals are attributed to the *LC* phase. The pronounced difference in the apparent velocity indicates that the boundary between the layer passed by the *Pg* and the layer passed by the *LC* phase (*i.e.*, the boundary between upper and lower crust) is deeper underneath the western part of the model than underneath the eastern part of it. Between 75 km and 100 km offset a secondary retrograde phase labeled *PcP* (apparent velocity ~6.6-6.7 km/s) is present which can be explained as a wide-angle reflection from the base of the upper crust. Onsets about 300-400 ms after the *LC* between 150 and 220 km offset are correlated as *PmP(1)* phase. They are rather diffuse, indicating a very weak continental Moho with low impedance contrast. Between 130 km and 180 km offset another secondary phase (*PmP(2)*) was observed. Its bulk apparent velocity is 7.7 km/s. The depth of the reflection points of this phase is about 45 km underneath the Coastal Cordillera. This phase is attributed to the oceanic Moho of the Nazca Plate.

SHOT 3

Shot 3 was fired from the Pacific Ocean about 20 km offshore (Fig. 3A). The observations are nearly equivalent to those from shotpoint 2. The *Pg*, *LC*, *PcP*, *PmP(1)*, and *PmP(2)* phases are observed in the same offset ranges. The most significant difference from the section of shot 2 is the observation of pronounced amplitudes along the *PmP(2)* branch at

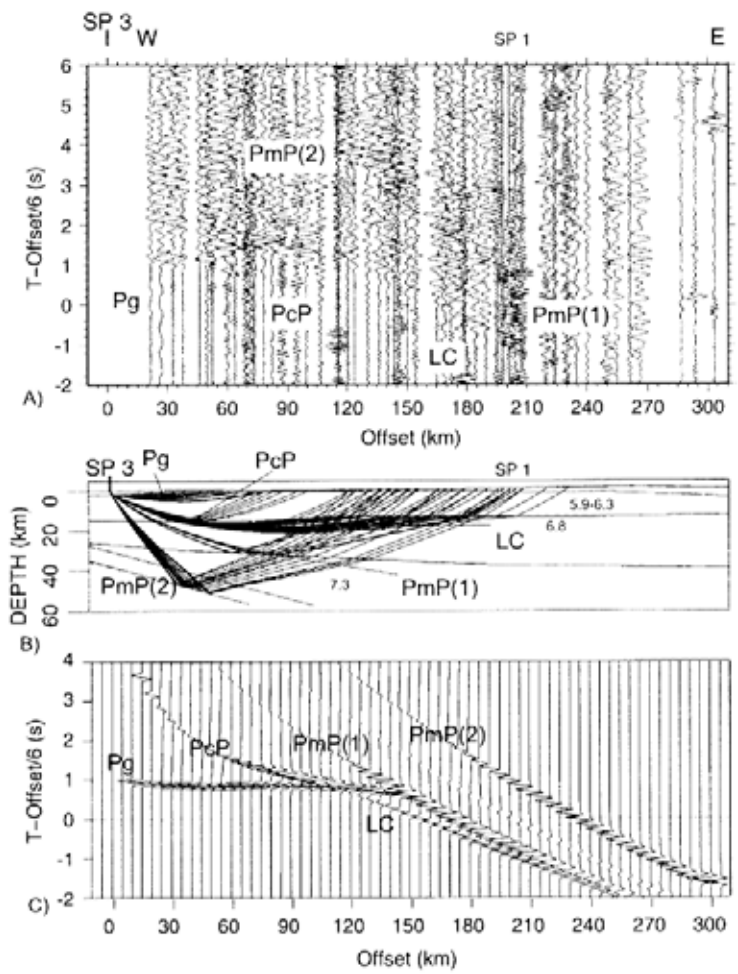

FIG. 3. **A)-** Shot section from the shotpoint 3 (Pacific Ocean). The data has been bandpass-filtered 2-12 Hz and reduced with 6 km/s. Grey lines denote the modeled traveltimes of the phases which had been picked in the section; **B)-** ray-diagram of the correlated phases. Numbers in the ray-diagram indicate P-wave velocities in km/s; **C)-** ray-theoretical seismogram based on the final velocity model.

130 to 150 km offset which should be still in the undercritical range of the phase for this model as suggested by the synthetic seismogram (Fig. 3C). At such a relatively low offset they are only visible in the section of shot 3 which suggests that this is rather a feature of a strongly two- (or even three-) dimensional lithosphere than of a layering of high- and low-velocity units, which would be the implication using a one-dimensional model and what could be concluded if all sections from the offshore shots showed the same feature. The sections from SP 2.1 and SP 4 show only weak indications of the *PmP(2)*-phase. This variation of the *PmP(2)*-onsets on the shot sections is not reconstructed by the synthetic seismograms which show a more stable behavior of the *PmP(2)*-phase on the three shot sections 2.1, 3, and 4. It may be assumed, that mere ray-theoretical modeling is not appropriate to explain the observations, because small scale heterogeneities of the oceanic Moho would have to be accounted for, which cannot be modeled using the high frequency approximation of the ray-tracing method.

SHOT 4

Shotpoint 4 is located in the Pacific Ocean about 10 km offshore (Fig. 4). The shot was recorded between 13 km and 295 km offset eastward. Probably due to increased traffic noise at the time of this shot (Sunday afternoon local time, all other shots were observed on Sunday in the early morning when there was much less civilization noise) the signal-noise ratio

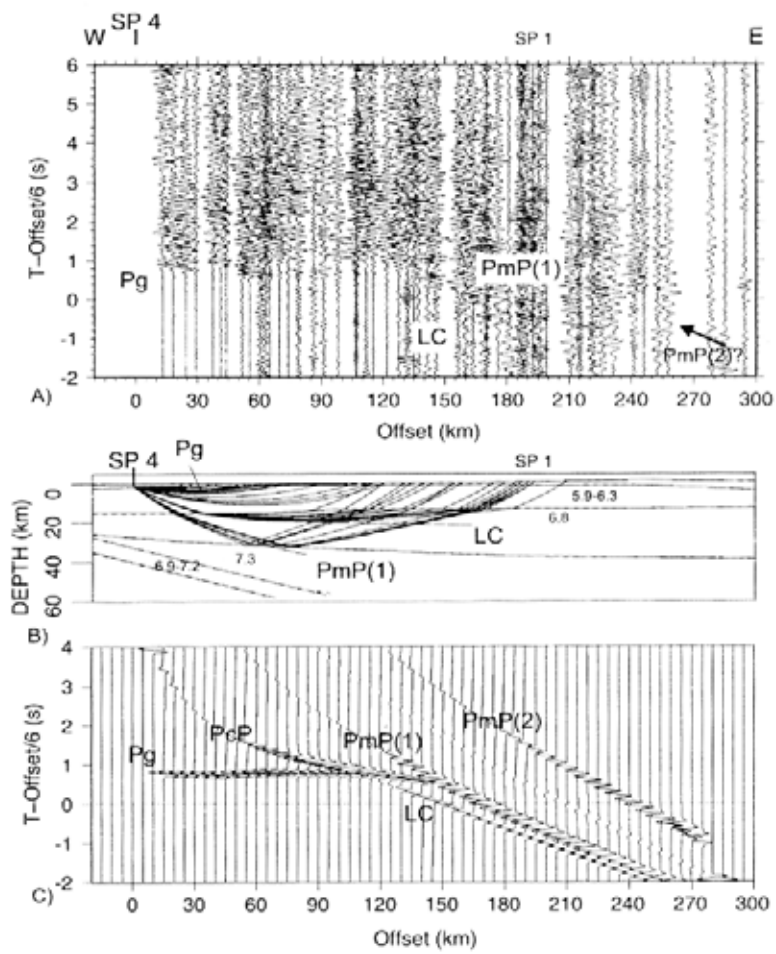

FIG. 4. **A)-** Shot section from the shotpoint 4 (Pacific Ocean). The data have been bandpass-filtered 2-12 Hz and reduced with 6 km/s. Grey lines denote the modeled traveltimes of the phases which had been picked in the section; **B)-** ray-diagram of the correlated phases. Numbers in the ray-diagram indicate P-wave velocities in km/s; **C)-** ray-theoretical seismogram based on the final velocity model.

is considerably worse than that of the sections 1 to 3. The first break traveltimes have been correlated according to the other offshore shot sections 2 and 3. The Pg phase is present from 13 km to 120 km offset at 6 km/s bulk apparent velocity. The *LC* phase is correlated from 120 km to 210 km offset at 7.1 km/s apparent velocity. The retrograde *PmP(1)* phase is observed from 120 km to 200 km offset. Either due to the bad signal-noise ratio, or due to small scale heterogeneities of the deep reflectors, the *PcP* and *PmP(2)*-phases were not correlated on the section, but ray-theoretically modeled (Fig. 4c). Onsets at ~250 km offset may be interpretated as *PmP(2)* but were not used for modeling (see arrow in Fig. 4a).

TRAVELTIME MODELING

The vertical component recordings of the shots were used to determine a P-wave velocity model of the area covered by the data. The first break traveltimes were correlated and the bulk velocity distribution of the upper crust was determined based on these traveltimes using two-dimensional ray-tracing (Zelt and Smith, 1992). A list of the phase correlations and modeling errors is given in table 1. Then, secondary phases were correlated and their traveltimes were used to determine velocity structure below the part of the model not covered by the primary arrivals.

The model derived from the traveltimes after trial-and-error ray-tracing was assessed with several methods in order to determine the width of the error bars for the model parameters.

A perturbation analysis for the velocities as derived from the traveltime correlations was performed. Furthermore, modeling of the seismic amplitudes (Zelt and Ellis, 1988), and gravity modeling after conversion of the velocity model into a density model were carried out in order to check the derived model with independent observations.

TABLE 1. LIST OF PHASES CORRELATED IN THE SHOT SECTIONS AND THEIR RMS TRAVELTIME.

List of correlated and modeled phases

Shot	Pg (rms)	LC (rms)	PcP (rms)	PmP (1) (rms)	PmP (2) (rms)
1	23 (71 ms)	11 (156 ms)	3 (189 ms)	5 (137 ms)	-
2	13 (50 ms)	21 (130 ms)	5 (156 ms)	9 (58 ms)	11 (247 ms)
3	11 (112 ms)	20 (192 ms)	6 (109 ms)	6 (195 ms)	13 (185 ms)
4	14 (113 ms)	11 (210 ms)	-	8 (172)	-
All	61 (87 ms)	63 (171 ms)	14 (146 ms)	28 (145 ms)	24 (216 ms)

The numbers indicate the number of traveltime picks and root-mean-square traveltime error (in brackets).

The velocity model (Fig. 2) derived from modeling of the observed traveltimes and amplitudes of the correlated phases consists of the following layers:

The first layer represents the varying thickness of (unconsolidated) sediments in the sedimentary basins (Valdivia Basin offshore (González, 1989) and Neuquén Basin at the eastern end of the model (Vergani *et al.*, 1995)). The authors modeled its P-wave velocity (v_p) between 2.0 and 5.8 km/s. The thickness of the layer reaches up to 5 km in the Neuquén

Basin. Seismic reflection observations and drilling cores are available for the sedimentary basins showing strong variation of the depth of the basement. The thickness of the Valdivia Basin sediments reaches up to 1.6 km (González, 1989). The sedimentary infill in the depocenter of the Neuquén Basin is at least 7 km thick (Vergani *et al.*, 1995). Due to the large distance between the offshore shots and the reverse shot in the Main Cordillera, the exact structure of the sedimentary layer is not well constrained along the whole profile, and the velocity values given above were indirectly inferred. The layer thickness was kept constant, consistent with literature values, and the velocity of the first layer was chosen such that the traveltime curves of deeper phases were not shifted with respect to the observed traveltimes.

The second layer, the crystalline upper crust, is crossed by rays of the *Pg* phase which constrains v_p within a narrow range (see estimation in the next section). The thickness of this layer is 15 km in the western part of the model and 10 km underneath the Main Cordillera. The thickness of this layer increases towards the eastern end of the profile where its total thickness is not resolved. v_p is 5.9 to 6.3 km/s, indicating felsic to intermediate composition.

The third layer, the lower crust, is constrained by rays of the *LC* phase. As the apparent velocities of this phase are higher on the shot sections from the offshore shots 2, 3 and 4 than on the shot section from shot 1, the upper boundary of this layer is modeled as dipping from east to west. v_p in this layer is 6.6 km/s to 6.9 km/s, indicating intermediate to mafic composition. The lower boundary of this layer is constrained by onsets of the *PmP(1)* wide-angle reflections. The reflection points of this phase are at roughly 25-30 km depth underneath the fore-arc.

The fourth layer is modeled as a wedge-shaped structure between the third and the fifth layer with v_p between 7.2 km/s and 7.3 km/s underneath the fore-arc. The exact velocity under the arc is not resolved as no *PmP* and *Pn* observations were made on the section from shot 1. The velocity and thickness of this layer is not directly constrained by refracted arrivals, the positive velocity contrast to the third layer is inferred from the existence of the *PmP(1)* arrivals. As these arrivals are relatively diffuse in the sections from the shotpoints in the Pacific Ocean with respect to the *PmP(2)* arrivals and mantle-type P-wave velocities (more than 7.6 km/s) at 25-30 km depth underneath the fore-arc would result in completely different traveltime curves and amplitudes, a velocity contrast weaker than a typical Moho-transition has been assumed for the fore-arc. The low seismic velocities in this part of the model exclude a 'normal' continental mantle. They may be caused either by serpentinization of continental mantle (Giese *et al.*, 1999), or the presence of sediment, which was subducted from the trench and underplated below the fore-arc (Díaz-Naveas, 1999).

Below the fourth layer the authors modeled a velocity inversion at 40-50 km depth below the fore-arc. The thickness of this layer is 7 km, the eastward dip is about 15°, and v_p increases from 6.9 to 7.2 km/s. This layer, as well as the fourth layer above is only passed by the rays of the *PmP(2)* phase which has strong amplitudes from 130 km offset eastward in the Pacific shot sections 2 and 3 and which indicates a strong positive velocity contrast at the lower boundary of the fifth layer. Due to the depth range of the reflection points of the *PmP(2)* phase the fifth layer is modeled as the subducting oceanic crust. Its thickness and velocity structure is inferred from seismic reflection data from the Chilean continental margin in the investigation area (Bangs and Cande, 1997; Díaz-Naveas, 1999) and from the nearest regions northward covered by seismic refraction data (Flüh *et al.*, 1998; Zelt *et al.*, 1999). The reflection points of the *PmP(2)* phase correspond to the Moho of the oceanic crust. The exact P-wave velocity of the oceanic mantle is not resolved due to the lack of *Pn* (refracted wave through the upper mantle) correlations. In correspondence to other velocity models of this region (*e.g.*, Flüh *et al.*, 1998) v_p of the mantle is 8 km/s in the model. The earthquake hypocenters plotted in figure 2 have been derived from the P- and S-wave traveltimes of earthquakes observed by the local network (Bohm *et al.*, 2002). Seismicity at 73°W and 40-50 km depth correlates well with the inferred location of the oceanic crust. The eastward dip of the oceanic Moho is also confirmed by receiver function imgages using teleseismic earthquake recordings along the ISSA transect (X. Yuan, oral communication, 2001).

ASSESSMENT OF THE MODEL

The velocity model presented together with estimations of the uncertainty of the model parameters can only be as good as the traveltime picks. When using traveltimes of different phases with differing pick uncertainties the normalized traveltime error χ^2 is used to assess the quality of the model. χ^2=1.0 indicates that an optimum fit between observed traveltimes and modeled traveltimes has been reached. $\chi^2 < 1$ indicates that there may be an overcorrection in the model, *i.e.*, it is not sure whether the structures inferred from the traveltimes are justified by the data or merely produced by possible pick errors. When deriving a model from real data it is realistic to allow a value of χ^2 slightly larger than 1 (*e.g.*,

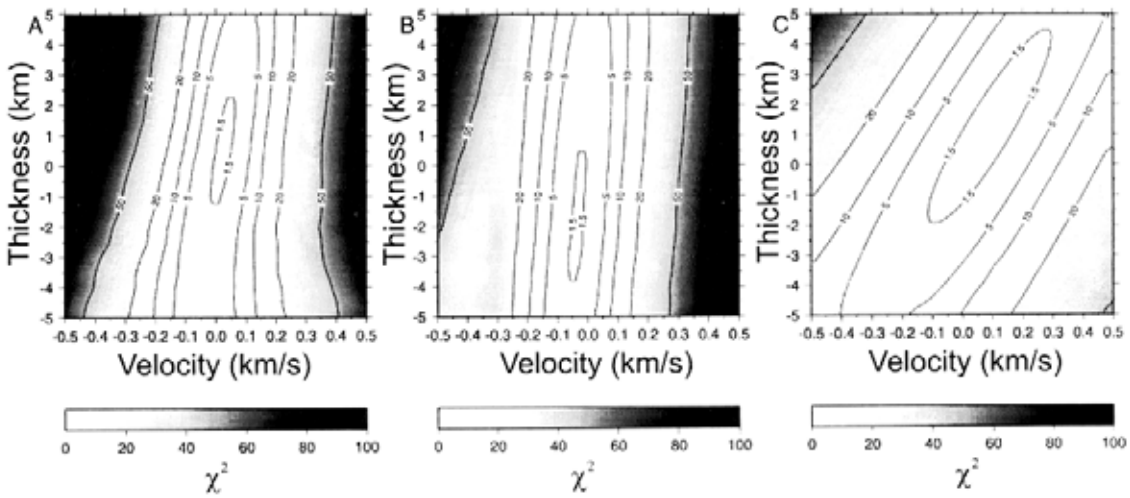

FIG. 5. 1-D perturbation analysis of upper continental crust **A**; lower continental crust **B**, and below the lower continental crust **C.** The contour plots show the normalized mean-squared traveltime error in dependence on velocity and thickness perturbation of the respective layers. Due to the presence of refracted and reflected phases for upper and lower crust the trade-off is very small (**A** and **B**); contrary to the part of the model between lower continental crust and oceanic Moho, which is passed by reflected phases only (**C**).

1.5) in order to account for several possible errors which are difficult to quantify (*e.g.*, side (3-D) effects, unresolved heterogeneities by rough parameterization, anisotropy, etc.).

The seismic refraction experiment was designed in order to deliver bulk velocity and structural information on the crust of the upper plate mainly. In order to determine the 'model space', a perturbation analysis was performed. The result is a 2-D distribution of the normalized traveltime error χ^2 in dependence on velocity and thickness perturbation. The perturbation is performed in one dimension in order to investigate the overall trade-offs between thickness and velocity of the layers.

The perturbed parameters are the thickness of the layer and its velocity at all nodes. In figure 5 the normalized traveltime error χ^2 is plotted depending on the perturbation of the thickness and v_p at all nodes of the upper crust, the lower crust, and the layer below. Only the phases which have their turning points in the respective layer or at its lower boundary are used for the test. In the upper crust the velocity is well constrained by the *Pg* phase, its thickness by the *PcP* phase (Fig. 5A). Assuming that the $\chi^2 = 1.5$ isoline marks the model space, v_p may not vary more than ± 0.05 km/s. The thickness of the layer may be reduced or increased by not more than 1-2 km.

The structure of the lower crust is constrained by the *LC* phase. The P-wave velocity may not be perturbed more than±0.05 km/s, the thickness of the layer is constrained by the traveltimes of the *PmP(1)* phase and may not vary more than 1-4 km. The trade-off values of velocity and depth are low because there are refracted and reflected phases constraining the model in the upper part. If only short traveltime branches of reflected phases were present, the trade-off would be much higher, which is the case for the lower part of the model (Fig. 5B).

Thickness and velocity of the layer below the lower crust are constrained by the *PmP(2)* phase. In the data it can be recognized that the picks of this phase are relatively unclear. Here a pronounced trade-off between velocity and thickness of the layer (*i.e.*, depth of the discontinuity where the *PmP(2)* rays are reflected) is present. Thickness and velocity may be decreased or increased by, at least, 2-4 km and 0.2 km/s, respectively (Fig. 5C). The perturbation was only performed in one dimension, not allowing single nodes to vary distinctly within one layer. Due to the rough spatial sampling of the shotpoints the actual uncertainty of the interval velocities and depth of the layer boundaries is probably higher.